Int. J. Electrochem. Sci., 13 **(2018)** 8575 – 8588, doi: 10.20964/2018.09.60

International Journal of
ELECTROCHEMICAL
SCIENCE
www.electrochemsci.org

Two-Dimensional MnO_2/reduced Graphene Oxide Nanosheet as a High-Capacity and High-Rate Cathode for Lithium-Ion Batteries

Tong Chen, Yirong Zhou, Junxi Zhang[*] *and Yongjie Cao*

Shanghai Key Laboratory of Material Protection and Advanced Material in Electric Power, Shanghai University of Electric Power, Shanghai, 200090, China
[*]E-mail: zhangjunxi@shiep.edu.cn

Received: 11 June 2018 / *Accepted:* 10 July 2018 / *Published:* 5 August 2018

Two-dimensional MnO_2/rGO nanocomposite has been synthesized by a facile wet chemical method at low temperature. Ultrathin layered MnO_2 nanosheets were well-dispersed and tightly attached on the surface of reduced graphene oxide (rGO) sheets. Owing to a special laminar structure and higher electrical conductivity of rGO, the lithium ion diffusion and the electronic transport into the MnO_2/rGO nanocomposites were increased, resulting in improved electrochemical performance as a cathode material in lithium-ion batteries. The first discharge-specific capacity of the layered MnO_2/rGO nanocomposites is 279.7mAh g^{-1} and maintains at 242mAh g^{-1} after 60 cycles at 0.1C. And the rate capability of MnO_2/rGO nanocomposites is 236.9, 230.2, 190.3, 159.7 and 121.4mAh g^{-1} at 0.1C, 0.2C, 0.5C, 1C and 2C, respectively. The excellent electrochemical performances highlight the two-dimensional layered MnO_2/rGO nanocomposites as a potential cathode material of lithium-ion batteries.

Keywords: two-dimensional materials; layered manganese dioxide; reduced graphene oxide; lithium-ion batteries.

1. INTRODUCTION

The rapid depletion of fossil fuels and environmental concerns has caused an ever-growing demand for technologies of advanced energy storage. Among the various energy storage systems, lithium-ion batteries (LIBs) is considered a promising candidate for the effective storage of energy due to its' their high energy density and long cycle life[1-3]. LIBs were entering rapid development of commercial applications. However, at the current stage, only about half of the Li atoms stored in the $LiCoO_2$, crystal lattice could be extracted in the process of recycling because of the limitation of the structure’s stabilization[4]. Similar with $LiCoO_2$, $LiFePO_4$ material also has the problem. In order to grope for the next generation s LIBs with higher energy and power densities, Nanotechnology has played an important role for the realization of advanced electrode materials with satisfactory capacity, higher cyclic stability and rate capability. Various 2D layer-structure materials have been synthesized and used as electrode materials for LIBs[5]. Among them, as the rise of graphene, two dimensional (2D) nanostructures have a huge impact on LIBs for its' larger surface-to-volume ratio and atomic-scale limiting thickness[6]. And the 2D nanosheets materials are highly desirable for obtaining superior electrochemical performance for its’ shorten the path for lithium ions and provide lager channels for lithium insertion on large exposed surfaces[7]. Recently, Dinesh and co-workers have synthesized the novel ultrathin Li_2MnSiO_4 nanosheets as high-capacity LIBs electrode. The nanosheets as cathode material exhibited a higher discharge capacity about 340mAh g^{-1} between 1.5V and 4.8V at a temperature of 45℃ and 0.02C[8]. Chen and cooperators reported a simple two-step method to synthesize carbon coated ultrathin anatase TiO_2 layer nanosheets. The ultrathin nanocomposites reveal high reversible capacities with excellent cyclic capacity retention at a relatively high charge/discharge rate[9]. Besides, such 2D transition metal chalcogenides (TMDs) materials with a single layer or few layers have been proposed to be used as anode materials in LIBs by reason of the abundant adsorption sites and short Li^+ diffusion channels, such as MoS_2[10-12], WS_2[13], VS_2[14], SnS_2[15], and TiS_2[16], etc. With the thickness of the 2D nanosheets materials decrease, the electrochemical performance can be improved greatly[11].

Among various 2D nanostructure potential cathode materials, manganese dioxide (MnO_2) is one of most promising and competitive materials for LIBs for its’ lower cost, rich abundance, non-toxicity and environmental friendly nature[17]. MnO_2 crystals are formed by edge-shared or shared MnO_6 octahedra. MnO_2 has various nanostructures with stacking of MnO_6 octahedra, such as one-dimensional (1D) tunnel-type (e.g. α-, β-, γ-MnO_2) and 2D layer-type (e.g. δ-MnO_2). Among the various MnO_2 structures, only birnessite δ-MnO_2 2D has a typical layered structure, which is formed by shared MnO_6 octahedra layers with water molecules and/or some kinds of alkaline metal ions in the interlayer regions[18]. Over the past years, birnessite δ-MnO_2 with such a layered structure has been successfully obtained and used as electrode material for LIBs and supercapacitors. Recently, Du and co-workers have synthesized layered structured δ-MnO_2 with a thickness of 5-10nm by a simply microwave-assisted hydrothermal method. The δ-MnO_2 cathode revealed high cycling stability and shown a discharge specific capacity of approximately 90mAh g^{-1} at 1C[19]. Zhu and colleagues proposed an ultra-rapid microwave-assisted strategy to prepare ultrathin birnessite $K_{0.17}MnO_2$ nanosheets with a thickness of 2nm. The electrode shown significant electrochemical properties compared with its’ bulk counterpart, suggesting a remarkably promising candidate for energy storage[20]. Deng and his workmates reported the adsorption and diffusion of Li ion on single-layer MnO_2 on the basis of first-principles calculations. The results proved that the single-layer or few-layers MnO_2 reveals excellent electrochemical properties in Li storage capacity and ion diffusion rate. compared with other 2D nanomaterials[21]. Although 2D layered MnO_2 attracts tremendous research interest, its poor electrical conductivity and volume expansion limits its practical applications in energy storage[22, 23]. Combining 2D layered MnO_2 with highly conductive materials, for instance activated carbons, carbon nanotubes and porous carbon can be an effective approach in solving the problems[24-26].

Herein, we choose layered birnessite MnO_2 to achieve that 2D material have superior electrochemical properties in energy storage. We have designed a simple route to synthesize ultrathin 2D MnO_2/rGO nanocomposites with excellent electrochemical performance acted as cathode materials for LIBs via one step wet chemical reaction. The layered MnO_2 nanosheets have loaded uniformly onto the reduced graphene oxide (rGO) and the nanocomposites also show a lamination morphology. The as-prepared ultrathin 2D MnO_2/rGO nanocomposites reveals high reversible specific capacity, higher cyclic stability and rate capability performance.

2. EXPERIMENTAL

2.1 Synthesis of MnO_2/rGO composites

All of the chemical reagents were in analytical grade and were directly used without any further purified. Graphene oxide (GO) was prepared by using flake graphite according to the Hummers method[27, 28], 2g graphite was added in 46mL H_2SO_4 (98 wt. %) at 0℃. Subsequently, 1.0g $NaNO_3$ was added gradually. Under continuous vigorous stirring, 6.0 g $KMnO_4$ was slowly added and kept the mixture temperature below 15℃ through ice water bath. The mixture was first stirred at below 15℃ for 30min and then stirred at below 35℃ until it turned to brown paste. After adding 100mL deionized water, the mixture was transferred to a 98℃ water bath with continuous stirring for 30min. Then, the mixture was diluted to 240mL by deionized water. Finally, 10mL H_2O_2 (30 wt. %) was slowly added into the mixture solution. The obtained product was washed many times until pH value was 7 by using 5 wt. % HCl and deionized water, respectively, to remove the residual ions. After that, the obtained mixture was dried in an oven at -24°C for 12h to obtain brown GO powders. Reduced graphene oxide (rGO) is obtained using magnetic stirring of the as-prepared GO solution (0.3g as-prepared GO is dispersed in100mL deionized water by ultrasonic dispersion) and using sodium borohydride (0.1 M $NaBH_4$) as a reducing agent at 80°C. After 24h reaction times, the cooled suspension is washed by centrifuging at 10000 rpm for 20 minutes for three times[29-31].

The ultrathin MnO_2/rGO nanosheet composites were synthesized by using an easy one-pot wet chemical reaction. In a typical procedure, 375mL 0.02mol/L $KMnO_4$ aqueous solution was taken in a round-bottom flask. After that, 0.163g as-prepared rGO was dissolved in 100mL ethyl acetate by ultrasonic for 1h, then, the mixture was added into the $KMnO_4$ aqueous solution and kept heating by a water bath with continuous stirring, and under refluxing condition at 83℃. The MnO_2/rGO precipitate was formed at the bottom of the flask. Subsequently, the precipitate was centrifuged at 6000r/ min for 5 minutes and washed with alcohol for several times. Finally, MnO_2/rGO mixed precipitate was dried in a vacuum oven at 70°C overnight. In contrast, the pure layered MnO_2 nanosheet was prepared using the same method and without adding rGO[32].

2.2 Materials characterization

The crystal structure information of the as-prepared samples was characterized by Bruker D8 Advance powder X-ray diffraction (made in Germany), using a *Cu Kα* radiation X-ray diffractometer ($\lambda = 0.1506$ *nm*) at a scan rate of 1°/min and step size of 0.01°. Morphologies of the as-prepared powders were characterized by scanning electron microscopy (SEM) using XL-30 FEG model. Transmission electron microscopy (TEM) images were achieved on a JEM-2100 transmission electron microscopy at an acceleration voltage of 200kV. The contents of interlayer water and rGO of the composites were determined using thermogravimetric analysis (TG, PerkinElmer). The temperature range was from room temperature to 750℃ at a heating rate of 2℃/min under an air atmosphere.

2.3 Electrochemical measurements

All the electrochemical measurements were evaluated in a standard CR2016 type coin cell. The composite cathode composed of 8:1:1 weight ratio active materials, carbon black (Alfa Aesar), and PTFE (polytetra-fluoroethylene, Sigma-Aldrich), which was milled by using high energy ball and ethanol as a solvent for 2 hours. The electrode composite loading average quality is 10mg and the area of the stainless steel electrodes was about 1cm^2. The cathode electrodes were prepared in vacuum oven drying at 120° C for 12h. The CR2016 coin-type cells were assembled in an argon filled glove box by using pure lithium slices as the counter electrode. To prepare the working electrode, 80 wt.% of active materials, 10 wt.% conductive material (acetylene black) and 10 wt.% PTFE were mixed by boll-milling. The loading mass of each electrode was 10mg. Then CR-2016 type coin cells were assembled in an Ar-filled glove box using glass-fiber as separators, and 1 mol L^{-1} $LiPF_6$ in a mixture of ethylene carbonate and diethyl carbonate (EC/DEC 1:1 by volume) solution was used as the electrolyte. Galvanostatic cycling tests were performed in the range of 2.0 V to 4.0 V, using a Land CT2001A battery test system (Wuhan Land, China). Electrochemical impedance spectroscopy (EIS) and cycling voltammetry (CV) tests were performed on an electrochemical work station (Chenhua CHI660, Shanghai, China) between 2.0V and 4.0V at the room temperature (25℃). CV scanning rate was 0.1mV/s. EIS perturbation signal was 5mV, and the frequency range was from 0.01Hz to 100 kHz.

3. RESULTS AND DISCUSSION

3.1 Growth mechanism of 2D MnO_2/rGO nanosheets

Previous studies have reported the electrochemical characteristics of MnO_2 due to its' particular crystallographic properties, while the layered-structure birnessite type δ-MnO_2 is considered as a promising phase for the applications in energy storage[33, 34]. Herein, we introduce rGO in the synthesis to improve the electrical conductivity. Aqueous $KMnO_4$/ethyl acetate (well dispersed with rGO) in a bottom flake was heated at 83℃ on a water bath under refluxing condition. A simple chemical reaction takes place in two steps. At the interface of the liquid phase, ethyl acetate is hydrolyzed slowly to forms ethanol and acetic acid under refluxing conditions. The as-prepared ethanol reacts with $KMnO_4$ and the brown MnO_2 forms on the surface of the rGO, due to rGO has a large specific area and it could facilitate the growth of MnO_2, and $KMnO_4$ reacts with ethanol at the water-organic boundary, in favor of the formation of ultrathin layered MnO_2 nanosheet. The reaction can be expressed as follows:

$$CH_3CO_2C_2H_5+H_2O \rightarrow CH_3CO_2H+CH_3CH_2OH \quad (1)$$

$$KMnO_4+CH_3CH_2OH \rightarrow KMnO_2+CH_3CO_2H \quad (2)$$

3.2 Physical characterization of 2D MnO_2/rGO nanosheets

Fig.1 (a) displays the powder XRD patterns of the pure MnO_2 and MnO_2/rGO composites. All of the pure MnO_2 powder diffraction peaks could corresponding to a monoclinic birnessite phase (JCPDS No. 80-1098), which is composed of edge-shared MnO_6 octahedra layers with water molecule and K^+ cations in the interlayer space.[19a] As shown in **Fig.1 (a)**, the pure MnO_2 and MnO_2/rGO composites display four characteristic peaks centered at 12.5°, 25°, 37° and 66.2°, that correspond to (001), (002), (20l) and (02l) basal reflections, respectively[35]. The characteristic diffraction peak at 26° for rGO was overlapped with the characteristic peak of MnO_2 around 25°[26]. Both of prepared materials gave a poorly resolved diffraction pattern, indicating that the pure MnO_2 and MnO_2/GO nanocomposites synthesized at low temperature had a lower crystallinity. The results of XRD patterns show that the layered structure of MnO_2 is not changed by adding rGO.

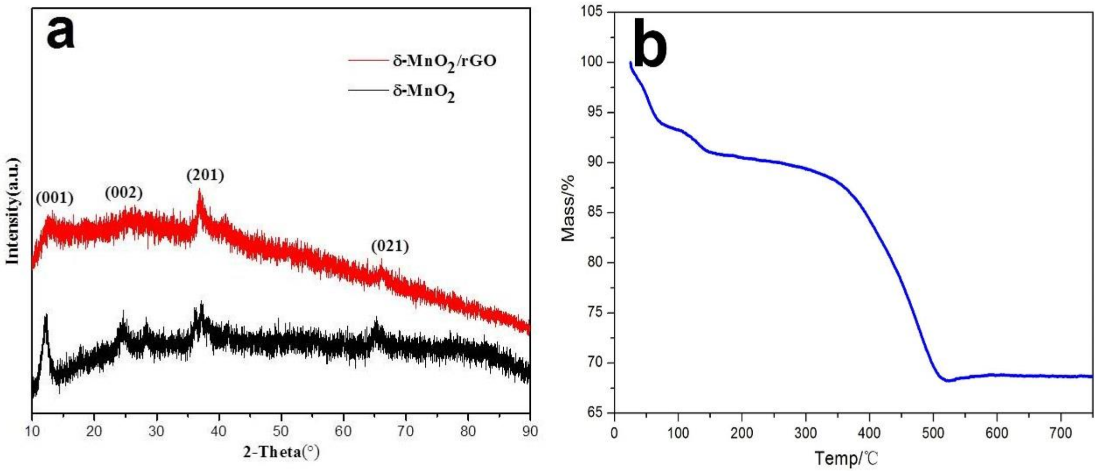

Figure 1. (a) The XRD patterns of MnO_2 and MnO_2@rGO composite; (b) TGA curve of the MnO_2@rGO composite

As shown in **Fig.1 (b)**, MnO_2/rGO powders lost about 7% of its weight between room temperature and 100℃, and the weight loss is caused by the removal of free water into material. And the process of 4% weight loss in the 100-300℃ which is related to the loss of interlayer water[24, 36]. In the temperature range 300-500℃, 22% weight loss is due to the oxidation of rGO in air[37, 38].

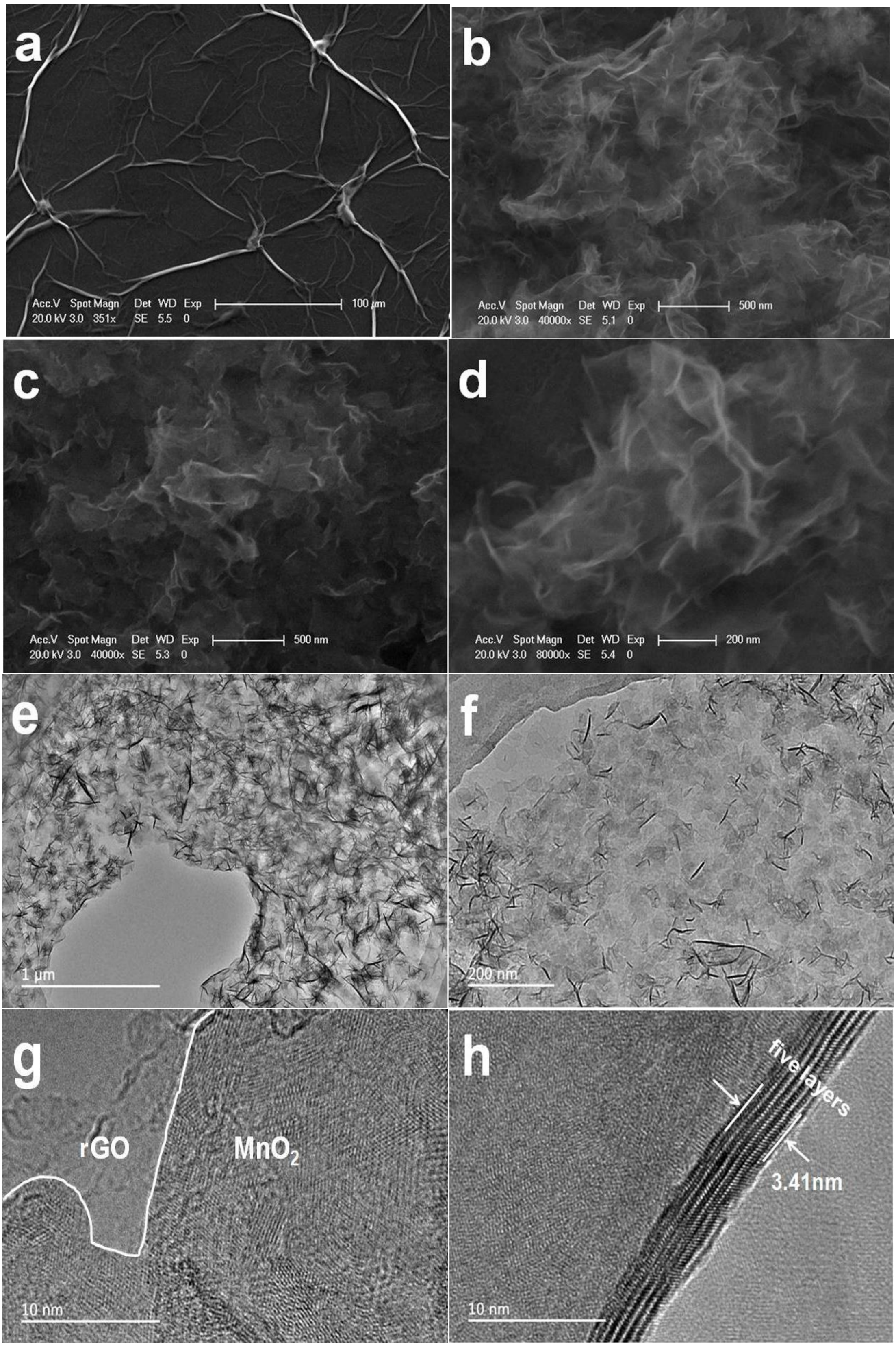
a
Acc.V Spot Magn Det WD Exp 100 μm
20.0 kV 3.0 351x SE 5.5 0
b
Acc.V Spot Magn Det WD Exp 500 nm
20.0 kV 3.0 40000x SE 5.1 0
c
Acc.V Spot Magn Det WD Exp 500 nm
20.0 kV 3.0 40000x SE 5.3 0
d
Acc.V Spot Magn Det WD Exp 200 nm
20.0 kV 3.0 80000x SE 5.4 0
e
1 μm
f
200 nm
g
rGO
MnO_2
10 nm
h
five layers
3.41nm
10 nm

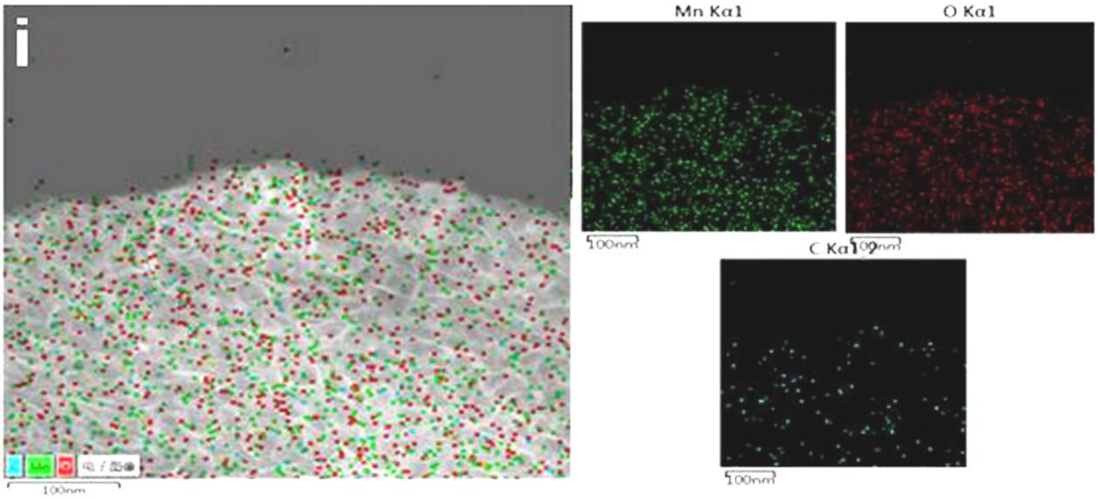

Figure 2. (a) SEM image of rGO; SEM image of pure MnO_2 (b) and MnO_2/rGO nanocomposite (c and d); (e, f, g and h) TEM images of MnO_2/rGO nanocomposite; (i) Element distribution mapping of Mn, O and C in MnO_2/rGO nanocomposite

Morphology and structure of layered birnessite-type MnO_2 and MnO_2/rGO composites were characterized by SEM and TEM. **Fig.2 (a)** displays a SEM image of obtained rGO by Hummers' method. The graphene sheet has typical characteristics and is basically consistent with the reports in the literature[27, 39]. **Fig.2 (b)** clearly shows that the pure MnO_2 shows a graphene-like 2D structure with a thickness of only few nanometers. **Fig.2 (c)** and **Fig.2 (d)** show the SEM images of MnO_2/rGO nanocomposites. It is obvious that the MnO_2 with sheet-like shape is homogeneously and tightly attached on the rGO surfaces. The corrugated nanosheets morphology can be easily accessed by lithium ions and the rGO can be effectively improving the conductivity of the composite. TEM images in a low magnification (**Fig.2 (e)**) further confirm the deposition of ultrathin MnO_2 nanosheets on the rGO thin films. And as it can be seen at a high magnification **(Fig.2 (f)**), the ultrathin sheet-like MnO_2 have an average diameter of approximately 100nm and distributed uniformly on the rGO surface, which is consistent with the SEM images. The high-resolution TEM (HRTEM) image of the edges of the MnO_2/rGO nanocomposites is shown in **Fig.2 (g)**. It can be observed evidently that MnO_2 nanosheets are anchored onto the rGO substrate. The interplanar spacing measured from the HRTEM image is 0.68 nm on average (**Fig.2 (h)**), which can be indexed as (001) lattice planes of birnessite type δ-MnO_2. **[35]** In addition, the thickness of about 3.41 nm is also determined directly by the HRTEM image of the curled edge of a single nanosheet. The uniform distribution of MnO_2/rGO nanocomposites was also investigated by TEM elemental mapping (**Fig.2 (i))**. Elemental mapping demonstrates that Mn, O and C are uniform distribution in sample.

3.3 Electrochemical performance of 2D MnO_2/GO nanosheets

The electrochemical impedance spectra of MnO_2/rGO electrode and MnO_2 nanosheet electrode and the equivalent circuit image are shown in **Fig.3**, both curves consist with a single semi-circle in a range of high to middle frequencies and a straight line at low frequency.

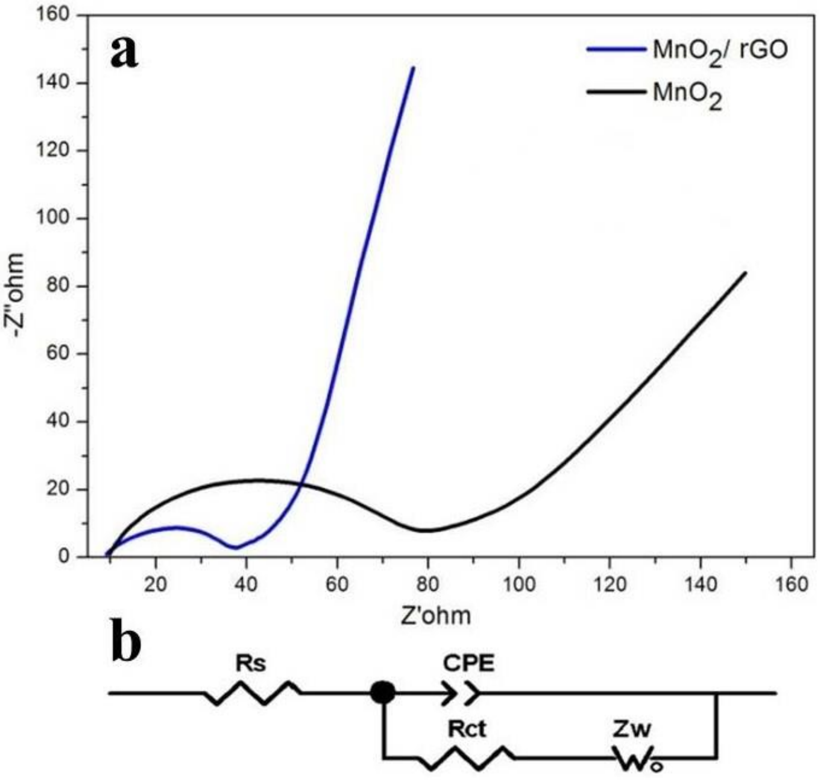

Figure 3. (a) The electrochemical impedance spectra and (b) equivalent circuit of MnO_2 nanosheet and MnO_2/rGO nanocomposite.

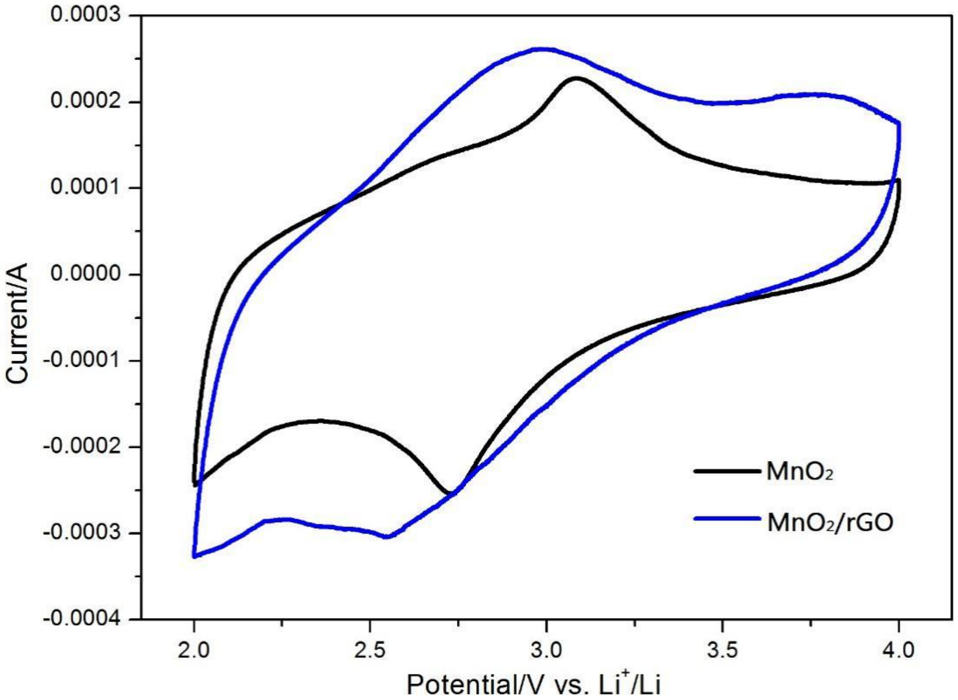

Figure 4. CV curves conducted at a scan rate of 0.1mV s^{-1} with potential window 2.0-4.0V for MnO_2 nanosheet and MnO_2/rGO composite

The parts of semi-circle and the straight line represent the process of lithium ions migration in the electrode[40-43]. The corresponding equivalent circuit model is also given in **Fig.3**. Rs represent electrolyte solution resistance, which CPE and Rct show the constant phase element and charge transformation, respectively. Zw represent the Warburg resistance of lithium ion diffusion. The Rct value of MnO_2/rGO nanocomposite electrode is 27.09 Ω, which is much lower than that of MnO_2 nanosheet electrode (78.08Ω). Although both LIBs cathode materials have similar active material/electrolyte interface during charging and discharging, rGO is added into the MnO_2/rGO nanocomposite to make electronic transmission much better[44,45].

The CV curves of MnO_2/rGO nanocomposite electrode and MnO_2 nanosheet electrode display in **Fig.4**. The two electrodes both show a coupled redox current peak located at 2.74/3.08V and 2.54/2.97V, respectively, corresponding to Li^+ intercalation and deintercalation in MnO_2. The two CV curves both have broad redox peaks, but compared with pure MnO_2, the curve of MnO_2/rGO exhibits a larger area, that is because rGO improved the conductivity and reduced the polarization of the electrode material, consequently, enhanced the specific capacity as LIBs cathode material.

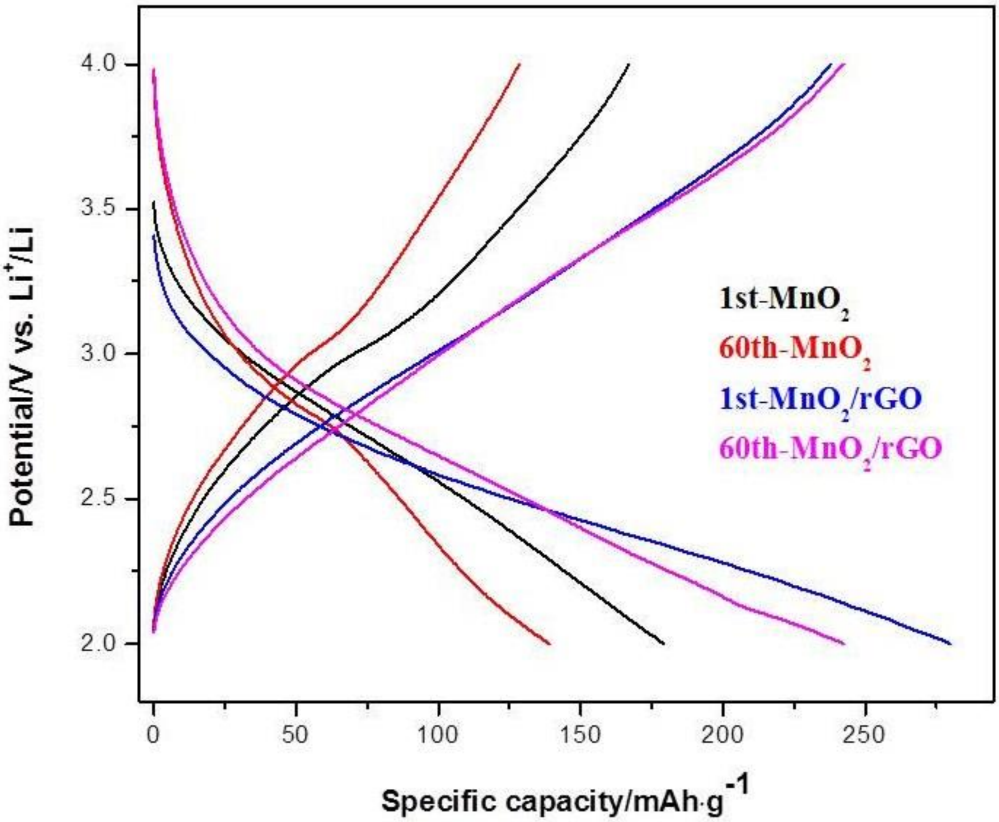

Figure 5. Discharge/charge profiles at 1st cycle and 60th cycles for MnO_2 nanosheet electrode and MnO_2/rGO composite electrode at 0.1 C

The charge/discharge voltage profiles of MnO_2/rGO nanocomposite electrode and pure MnO_2 nanosheet electrode at 1st and 60th as LIBs are shown in **Fig.5**. Both the 2D cathode materials reveal a monotonous voltage change without a significant voltage platform, which is well consistent with the results of CV measurement.

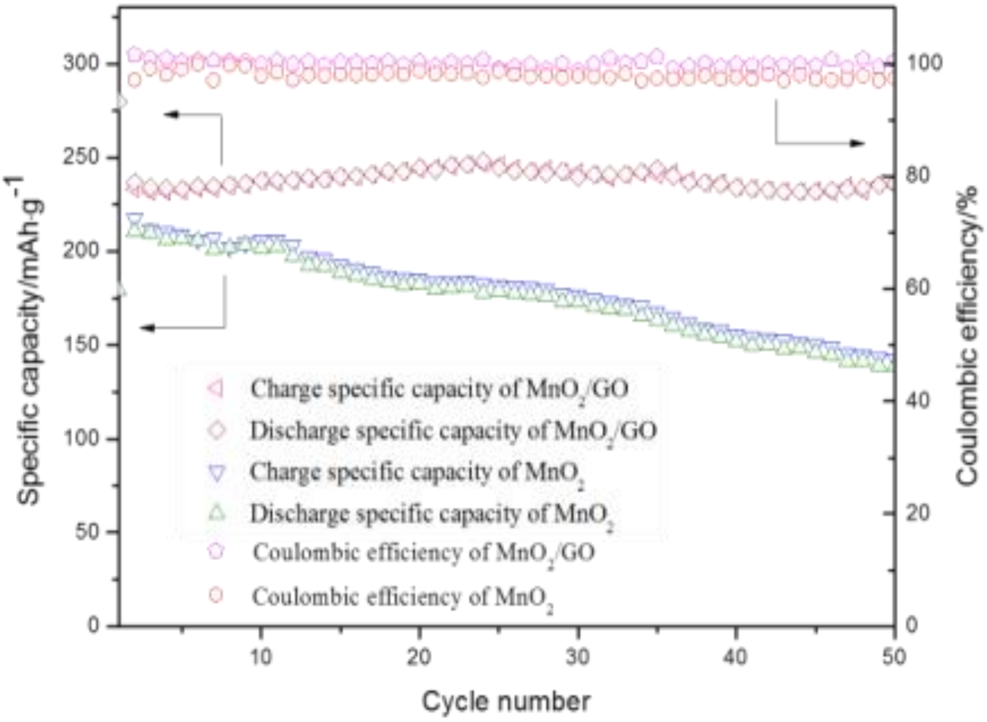

Figure 6. Cycling stability and the corresponding coulombic efficiency of MnO_2/rGO and MnO_2 electrode at 0.1C

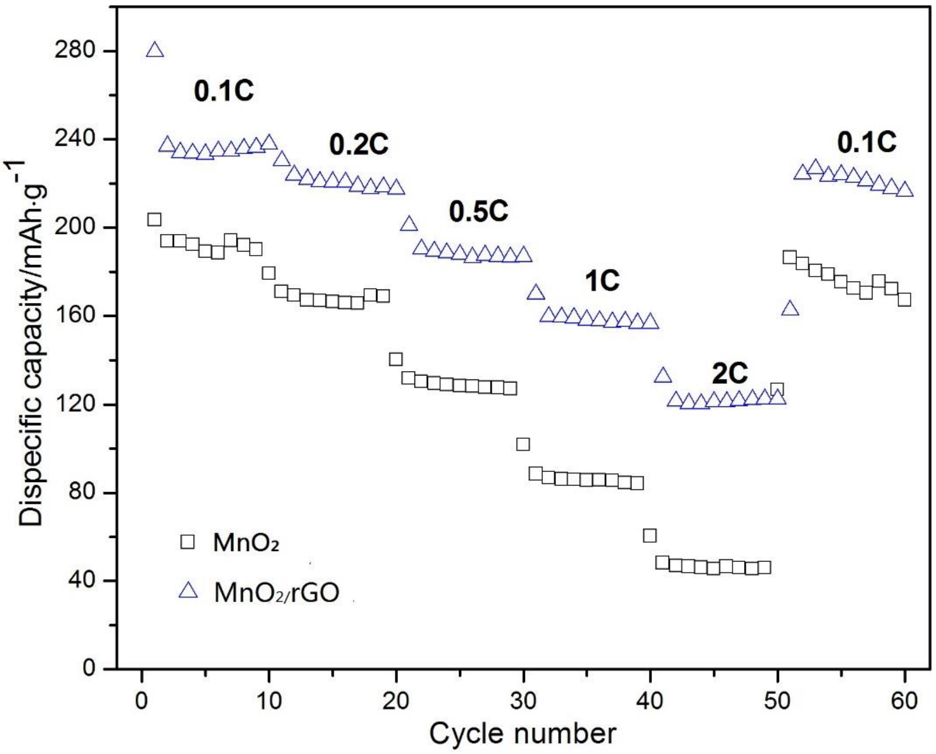

Figure 7. Rate capability curves of MnO_2/rGO nanocomposite electrode

The 1st cycle's charge and discharge specific capacities of MnO_2/rGO nanocomposite electrode are 278.6 and 244.7mAh g^{-1}, and 60th cycle's charge and discharge specific capacities are 242.3 and 242.2mAh g^{-1}, respectively. As a comparison, the MnO_2 nanosheet electrode's charge and discharge specific capacities are 189.3 and 184.5mAh g^{-1}, 153.1 and 149.6mAh g^{-1}, respectively. It can be observed that the MnO_2/rGO nanocomposite cathode revealed an obviously higher discharge capacity than pure MnO_2 nanosheet cathode.

Fig.6 compares the cyclic stability and corresponding coulombic efficiency of the MnO_2/rGO cathode with the MnO_2 nanosheet electrode as LIBs. Both electrodes were cycles between 2 and 4V at 0.1 C for 50 cycles.

According to the profiles, the first discharge capacity of MnO_2 electrode is 206.8mAh g^{-1} and the specific discharge capacity of the nanosheet maintains about 149.6mAh g^{-1} after 50 cycles, only 72.3% capacity retention. As for MnO_2/rGO nanocomposite electrode, the first discharge capacity is up to 279.7mAh g^{-1}, much higher than MnO_2 nanosheet electrode, and after 50 cycles the discharge specific capacity maintains approximately 249.9mAh g^{-1}, 89.3% capacity retention. Both of the cathode materials have excellent coulombic efficiency maintains almost 100%. The results clearly show that the MnO_2/rGO nanocomposite electrode, as a LIBs cathode material, has a much higher specific discharge specific capacity than MnO_2 nanosheet electrode for LIBs and could be seen that MnO_2/rGO electrode shows excellent cycling stability compared with MnO_2 nanosheet electrode.

Table 1. The cycle performance of δ-MnO_2/rGO LIBs cathode material compared with other previously MnO_2 and MnO_2 composites cathode material.

Cathode material	Voltage window (V)	Cycle performance	References
$K_{0.17}MO_2$	1.5-4.3	167mAh g-1 for 100 cycles at 0.1C	[20]
α-MnO_2	2.0-4.0	75mAh g^{-1} for 100 cycles at 0.1C	[40]
Li_xMnO_2	2.0-4.0	266mAh g^{-1} for 250 cycles at 0.1C	[41]
γ-MnO_2/MCNTs	1.5-4.0	150mAh g^{-1} for 200th cycle at 1C	[42, 43]
δ-MnO_2/MCNTs	1.5-4.0	99mAh g^{-1} for 100 cycles at 0.1C	[42]
δ-MnO_2	2.0-4.0	149mAh g^{-1} for 50 cycles at 0.1C	**This work**
δ-MnO_2/rGO	2.0-4.0	249.9mAh $g^{-1}$for 50 cycles at 0. 1C	**This work**
δ-MnO_2/rGO	2.0-4.0	159.7mAh $g^{-1}$for 10 cycles at 1C	**This work**

The rate capability performance of MnO_2 nanosheet electrode and MnO_2/rGO electrode are shown in **Fig.7**. The MnO_2/rGO nanocomposite electrode delivers reversible capacities of 236.9, 230.2, 190.3, 159.7 and 121.4mAh g^{-1} at 0.1C, 0.2C, 0.5C, 1C and 2C, which is much higher than pure MnO_2 nanosheet electrode, which has a reversible capacity of 193.9, 171, 130.3, 86.7 and 46.8mAh g^{-1} at 0.1 C, 0.2 C, 0.5 C, 1 C and 2 C, respectively. The cycle performance of δ-MnO_2/rGO nanocomposite is compared with other have reported LIBs cathode materials as shown in Table 1. As we can see in the table, δ-MnO_2/rGO cathode material of our study exhibits excellent cycle characteristic compared with other MnO_2 and their composite materials. The good cycle performance due to both δ-MnO2 and rGO have the unique 2D layered structure, and rGO has great electronic conductivity, that is easier to transport for electron. Additionally, the nanoscale layered δ-MnO_2/rGO sheet can offer between material and electrolyte interface reaction and accelerate the lithiation-delithiation process during batteries charge-discharge, because of the composite material has a larger specific surface area. As we studied, the MnO_2/rGO nanocomposite LIBs cathode has not only proved that has high reversible capacity and excellent cycling stability, but also has good rate capability performance.

4. CONCLUSIONS

In summary, ultrathin MnO_2 nanosheet is synthesized via a facile one step wet chemical reaction by using $KMnO_4$ as oxidation agent and ethyl acetate as reduction agent. Also, the rGO is used to improve electrical conductivity of MnO_2 nanosheet. The as-prepared MnO_2 nanosheet and MnO_2/rGO are applied as a cathode material of LIBs. The lithium-ion storage capability of the MnO_2/rGO is prominently enhanced comparing with the pure MnO_2 nanosheet. The first discharge capacity is up to 279.7mAh g^{-1}, and after 50 cycles the discharge specific capacity maintains approximately 249.9mAh g^{-1}, 89.3% capacity retention which are much higher than MnO_2 nanosheet electrode (206.8mAh g^{-1} maintains 149.6mAh g^{-1} after 50 cycles). In particular, compared with the rate capacity performance of MnO_2 nanosheet electrode, the MnO_2/rGO electrode keeps a reversible specific discharge capacity of 121.4mAh g^{-1} at 2C which is much higher than 46.8mAh g^{-1} at 2C. The excellent electrochemical performance of MnO_2/rGO electrode is due to its unique 2D layered structure and the high electrical conductivity of rGO, which could contain huge volume charge and enable a faster ion and electron transport. This 2D layered MnO_2/rGO nanocomposite could be prospective cathode materials for LIBs.This work also sheds insight into a novel method to large scale synthesis of 2D layered materials for other energy storage devices like secondary batteries or supercapacitors.

ACKNOWLEDGEMENT
This work was carried out with the financial support of the Shanghai Science & Technology Commission Project 13NM1401400 and the Project of Shanghai Science & Technology Commission (No. 14DZ2261000).

References

1. V. Etacheri, R. Marom, R. Elazari, G. Salitra and D. Aurbach, *Energy Environ. Sci.*, 9 (2011) 3243.
2. M. Armand and J.M. Tarascon, *Nature,* 451 (2008) 652.
3. Y. Gogotsi and P. Simon, *Energy Stora. Sci.*, 334 (2011) 917.
4. Y. Bai, H. Shi, Z. Wang and L. Chen, *J. Power Sources*, 167 (2007) 504.
5. P.G. Bruce, B. Scrosati and J.M. Tarascon, *Angew. Chem.*, 47 (2008) 2930.
6. M. Osada and T. Sasaki, *Adv. Mater.*, 24 (2012) 210.
7. J. Liu, X.W. Liu, *Adv. Mater.*, 24 (2012) 4097.
8. D. Rangappa, K.D. Murukanahally, T. Tomai, A. Unemoto and I. Honma, *Nano Lett.*, 12 (2012) 1146.
9. J.S. Chen, H. Liu, S.Z. Qiao, X.W. Lou, *J. Mater. Chem.*, 21 (2011) 5687.
10. K. Chang and W. Chen, *J. Mater. Chem.*, 21 (2011) 17175.
11. H. Hwang, H. Kim and J. Cho, *Nano Lett.*, 11 (2011) 4826.
12. T. Stephenson, Z. Li, B. Olsen and D. Mitlin, *Energy Environ. Sci.*,7 (2014) 209.
13. R. Bhandavat, L. David and G. Singh, *J. Phys. Chem. Lett.*, 3 (2012) 1523.
14. Y. Jing, Z. Zhou, C.R. Cabrera and Z. Chen, *J. Phys. Chem. C*, 117 (2013) 25409.
15. C. Zhai, N. Du and H.Z. Yang, *Chem. Commun*., 47 (2011) 1270.
16. C. Lin, X. Zhu, J. Feng, C. Wu, S. Hu, J. Peng, Y. Guo, L. Peng, J. Zhao, J. Huang, J. Yang and Y. Xie, *J. Amer. Chem. Soc.*, 135 (2013) 5144.
17. J. Cabana, L. Monconduit, D. Larcher and M.R. Palacin, *Adv. Mater.*, 22 (2010) 1170.
18. D.M. Robinson, Y.B. Go, M. Mui, G. Gardner, Z. Zhang, D. Mastrogiovanni, E. Garfunkel, J. Li, M. Greenblatt and G.C. Dismukes, *J. Amer. Chem. Soc.*, 135 (2013) 3494.
19. G. Du, J. Wang, Z. Guo, Z. Chen and H. Liu, *Mater. Lett.*, 65 (2011) 1319.
20. J. Zhu, Q. Li, W. Bi, L. Bai, X. Zhang, J. Zhou and Y. Xie, *J. Mater. Chem. A*, 1 (2013) 8154.
21. S. Deng, L. Wang, T. Hou and Y. Li, *J. Phys. Chem. C*, 119 (2015) 28783.
22. J. Chen, Y. Wang, X. He, S. Xu, M. Fang, X. Zhao and Y. Shang, *Electrochim. Acta*, 142 (2014) 152.
23. X. Guo, J. Han, L. Zhang, P. Liu, A. Hirata, L. Chen, T. Fujita and M. Chen, *Nanoscale*, 7 (2015) 15111.
24. H. Xia, M. Lai and L. Lu, *J. Mater. Chem.*, 20 (2010) 6896.
25. C.X. Guo, M. Wang, T. Chen, X.W. Lou and C.M. Li, *Adv. Energ. Mater.*, 1 (2011) 736.
26. S.W. Lee, C.W. Lee, S.B. Yoon, M.S. Kim, J.H. Jeong, K.W. Nam, K.C. Roh and K.B. Kim, *J. Power Sources*, 312 (2016) 207.
27. Y. Zhu, S. urali, W. Cai, X. Li, J.W. Suk, J.R. Potts and R.S. Ruoff, *Adv. Mater.*, 22 (2010) 3906.
28. S. Stankovich, R.D. Piner, S.T. Nguyen and R.S. Ruoff, *Carbon*, 44 (2006) 3342.
29. L.G. Guex, B. Sacchi, K.F. Peuvot, R.L. Andersson, A.M. Pourrahimi, V. Strom, S. Farris and R.T. Olsson, *Nanoscale*, 27 (2017) 9.
30. Václav Štengl, Jiří Henych, Petr Vomáčka and Michaela Slušná, *Photochemistry & Photobiology*, 89 (2013) 1038.
31. D. Yin, G. Huang, Q. Sun, Q. Li and X. Wang, *Electrochim. Acta*, 215 (2016) 410.
32. A.K. Sinha, M. Pradhan and T. Pal, *J. Phys. Chem. C*, 117 (2013) 23976.
33. S. Yang, X. Song, P. Zhang and L. Gao, *ACS Appl. Mater. Inter*, 5 (2013) 3317.
34. Y. Liu, X. Miao, J. Fang, X. Zhang, S. Chen, W. Li, W. Feng, Y. Chen, W. Wang and Y. Zhang, *ACS Appl. Mater. Inter*, 8 (2016) 5251.
35. H.T. Zhu, J. Luo, H.X. Yang, J.K. Liang, G.H. Rao, J.B. Li and Z.M. Du, *J. Phys.Chem. C,* 112 (2008) 17089.
36. F. Leroux and L.F. Nazar, *Solid State Ionics*, 100 (1997) 103.

37. G. Wang, J. Yang, J. Park, X. Gou, B. Wang, H. Liu and J. Yao, *J. Phys.Chem. C*, 112 (2008) 8192.
38. M. Kim, Y.H. wang and J. Kim, *J. Power Sources*, 239 (2013) 225.
39. G. Wang, X. Shen, J. Yao and J. Park, *Carbon*, 47 (2009) 2049.
40. T. Cetinkaya, M. Tokur, S. Ozcan, M. Uysal and H. Akbulut, I*nternational Journal of Hydrogen Energy*, 41 (2016) 6945.
41. S. Behboudi-Khiavi, M. Javanbakht, S.A. Mozaffari and M. Ghaemi, *Electrochim. Acta*, 261 (2018) 491.
42. S. Luo, S. Xu, Y. Zhang, J. Liu, S. Wang and P. He, *Journal of Solid State Electrochemistry*, 20 (2016) 2045.
43. D. Wang, L.M. Liu, S.J. Zhao, B.H. Li, H. Liu and X.F. Lang, *Physical chemistry chemical physics*, 15 (2013) 9075.
44. W. Devina, J. Hwang and J. Kim. *Chemical Engineering Journal*, 345 (2018) 1.
45. Y. Liu, S.J. Xu, S.M. Zhang, J.X. Zhang, J.C. Fan and Y.R. Zhou, *Journal of Materials Chemistry A*, 3 (2015) 5501.